Met. Mater. Int., Vol. 16, No. 5 (2010), pp. 761~766
doi: 10.1007/s12540-010-1010-y Published 26 October 2010

Oxidation of ZC63 Mg Alloys Reinforced with SiC Particles between 390 °C and 500 °C in Air

Dong Bok Lee*, Thuan Dinh Nguyen, and Young Jig Kim

School of Advanced Materials Science and Engineering, Sungkyunkwan University, 300, Cheoncheon-dong, Jangan-gu, Suwon-si, Gyeonggi 440-746, Korea

(received date: 22 February 2010 / accepted date: 7 June 2010)

The ZC63 magnesium alloys reinforced with 10 wt.% of SiC particles with an average particle size of 50 μm were cast. The fabricated SiC_p/ZC63 composite consisted of an α-Mg matrix, unreacted α-SiC particles, and an intergranularly formed CuMgZn compound. It was oxidized at 390 °C to 500 °C up to 5 h in air. The oxide scales were thin and compact below 430 °C, but became porous and loose above 450 °C. They consisted primarily of MgO and a small amount of Mg_3N_2. SiC particles were stable over the temperature range explored.

Keywords: metals, casting, oxidation, thermal analysis, magnesium

1. INTRODUCTION

Magnesium alloys are widely used as structural components in automobile and aerospace industries due to their low density, easy recycling ability, good weldability, damping property, castability, and abundance in oceans and ores [1-3]. However, their main drawbacks are inferior mechanical properties: low ductility at room temperature due to their hexagonal close-packed structure, plastic anisotropy, and a rapid decrease in yield stress and tensile strength at elevated temperatures. The mechanical properties can be increased by age hardening. Binary Mg-Zn alloys respond to age hardening. However, they suffer grain coarsening, limited deformability, and are susceptible to microporosity. The ternary addition of Cu markedly increases both ductility and response to age hardening [4,5]. A typical example is ZC63, whose composition is listed in Table 1. In the ZC63 magnesium alloy, Cu imparts a grain refining effect, and Zn provides good castability and ductility [6]. Nevertheless, the applications of magnesium alloys remain limited due to their insufficient strength and low abrasion resistance [7]. These drawbacks can be overcome by reinforcing the matrix with a stiffer ceramic phase such as SiC particles (SiC_p) [5,8]. SiC is the most popular because of its relatively high wettability and stability in a magnesium melt [7]. Recently, considerable efforts have been devoted to studying microstructure, mechanical properties, and fabrication of ZC63 magnesium matrix composites reinforced with SiC_p, viz., SiC_p/ZC63 [9-11].

Magnesium alloys are frequently exposed to oxidizing gases at high temperatures during manufacturing and utilization. They are highly susceptible to oxidation because of high reactivity of magnesium with oxygen. Among magnesium alloys, AZ91D (Mg-9Al-1Zn-0.13Mn, in wt.%) is the most widely used alloy, and therefore, its high-temperature oxidation behavior has been investigated extensively [12]. The AZ91D alloy starts to react with oxygen rapidly after approximately 30 min at 437 °C, resulting in accelerated weight gains. At temperatures higher than 507 °C, it is prone to ignition. However, high-temperature oxidation studies on ZC63 alloy and SiC_p/ZC63 composites are scarce, although it is an important factor during manufacturing, welding, and utilization at high temperatures. In this study, SiC_p/ZC63 composites were cast and oxidized isothermally between 390 °C and 500 °C in air. The aim of this study is to examine the oxidation of SiC_p/ZC63, which has not adequately been investigated before.

2. EXPERIMENTAL PROCEDURE

About 800 g of a commercial ZC63 alloy was melted in a steel crucible in a SF_6/CO_2 gas mixture using an electric resistance furnace. The alloy melt was rotated at a speed of 800 rev./min at 650 °C. The pre-heated α-SiC_p particles (98.5% purity with an average diameter of 50 μm) were added into the alloy melt with a feed rate of 10 g/min to 10 wt.%. A post rotation was conducted for 5 min, and then the SiC_p/ZC63 composite melt was cast into a steel mold.

The test coupons were cut from the ingots using a dia-

*Corresponding author: dlee@skku.ac.kr

Table 1. Chemical composition of ZC63 magnesium alloy (in wt.%)

Zn	Cu	Mn	Mg
6	2.8	0.5	rest

mond saw. Their surface was ground up to a 2000-grit finish with SiC paper and ultrasonically cleaned in acetone prior to oxidation. The coupons were oxidized isothermally at temperatures between 390 °C and 500 °C in atmospheric air using a muffle furnace or a thermogravimetric analyzer (TGA). The coupons were characterized by a scanning electron microscope (SEM), an optical microscope (OM), an X-ray diffractometer (XRD) with Cu-K_α radiation, and an Auger electron spectroscope (AES). A cross-sectional specimen for transmission electron microscope (TEM) was fabricated using a focused ion-beam miller (FIB) with a liquid-gallium-metal ion source and a maximum accelerating voltage of 30 kV. The TEM foil was examined in a TEM at 200 kV equipped with an energy dispersive spectrometer (EDS) with a spot size of 5 nm-diameter.

3. RESULTS AND DISCUSSION

Figure 1 shows the analytical results of the as-cast SiC_p/ZC63 composite. SiC_p was distributed uniformly in the matrix. It occupied approximately 9.8 % of the volume with an interfacial area of about 7.1 × 10^3 m^2/m^3, according to the point counting method (Fig. 1(a)). In Fig. 1(b), the matrix was etched with a solution of HNO_3: ethyl alcohol = 1: 20 (in volume). The average grain size of the ZC63 base alloy was 19.5 μm. The SEM image and the corresponding EDS line profiles of the matrix are shown in Figs. 1(c) and (d), respectively. Along the grain boundaries, all the alloying elements were segregated. The XRD pattern shown in Fig. 1(e) indicates that the SiC_p/ZC63 composite consisted of the α-Mg matrix as the major phase, unreacted α-SiC_p as the minor phase [11], and intergranularly formed CuMgZn as another minor phase. A CuMgZn compound was also found in the ZC63 [13] along with Mg-Cu-Zn-Y alloys [14,15]. Compounds such as $Mg(Zn,Cu)_2$ [1,5,10,11] or Mg(Zn,Cu) [1] or Mg_2Zn_3 [4,5] that were found in other Mg-Zn(-Cu) alloys were not found in this study. This difference in detected compounds may be attributed to different cooling rates after casting. The JCPDS numbers for the detected phases were inserted in the XRD pattern shown in Fig. 1(e).

Figure 2 shows the XRD patterns of the oxidized SiC_p/ZC63 composite. In Fig. 2(a), strong α-Mg peaks and weak peaks of SiC_p and CuMgZn were observed without any indication of oxides because of negligible oxidation at 430 °C for 5 h. In Fig. 2(b), MgO peaks came out owing to increment of oxidation temperature. However, the extent of oxi-

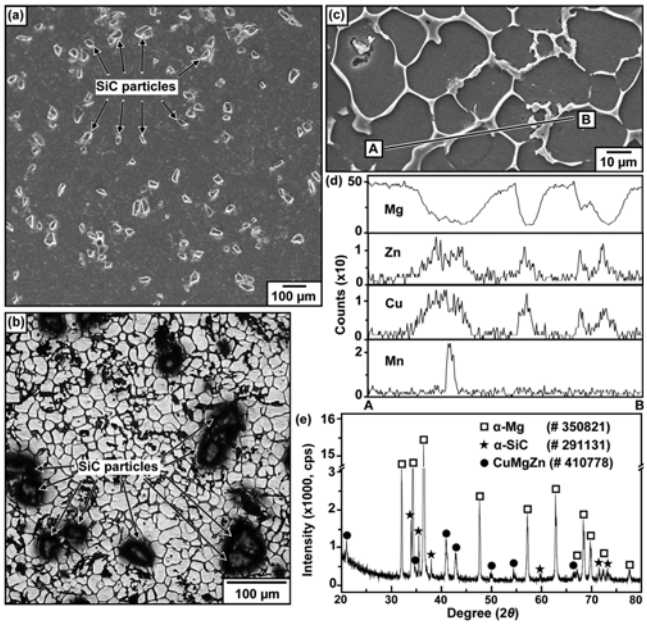

Fig. 1. As-cast SiC_p/ZC63 composite. (a) SEM microstructure (unetched), (b) optical microstructure (etched), (c) SEM microstructure (etched), (d) EDS lines profiles along A–B shown in (c), and (e) XRD pattern.

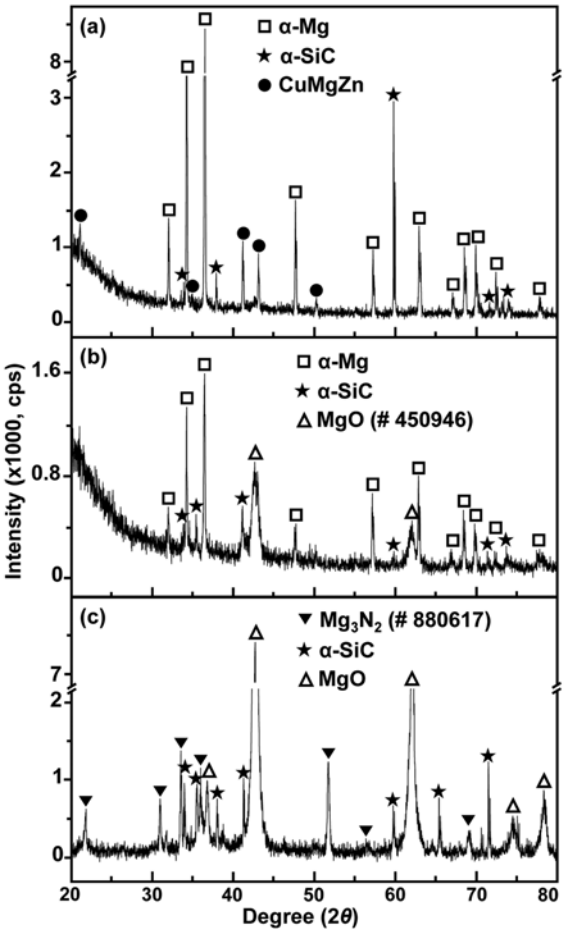

Fig. 2. XRD patterns of SiC_p/ZC63. (a) at 430 °C for 5 h, (b) at 450 °C for 5 h, and (c) 500 °C for 1 h.

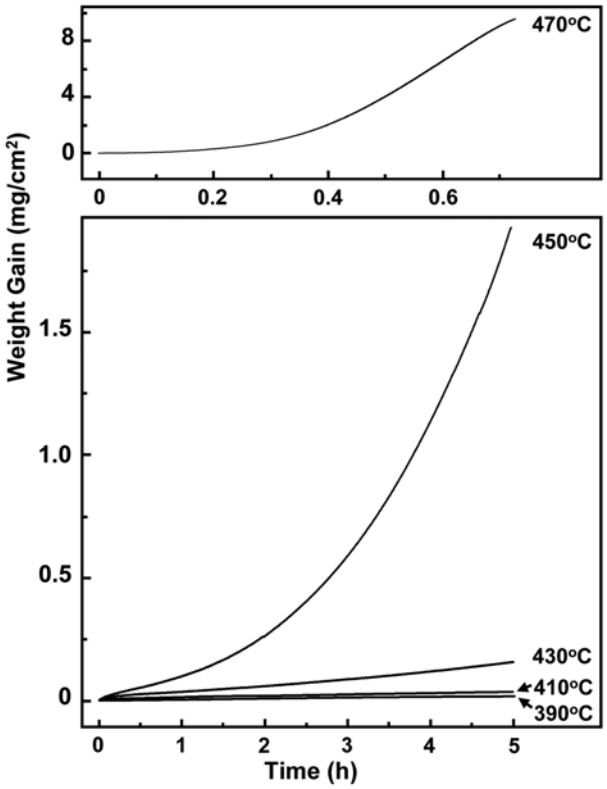

Fig. 3. Weight gain versus oxidation time curves of SiC_p/ZC63 at 390 °C, 410 °C, 430 °C, 450 °C, and 470 °C in air.

dation was still small so that α-Mg and SiC_p peaks were recognizable. The composite oxidized completely into powder when oxidized at 500 °C for 1 h, whose XRD pattern is shown in Fig. 2(c). This indicates MgO as the major phase, and Mg_3N_2 and SiC_p as the minor ones. In this study, MgO was always the main oxide, and SiC_p did not react with oxygen. Mg_3N_2 was formed by the reaction of nitrogen in air with Mg metal owing to its thermodynamic stability.

Figure 3 shows the isothermal-oxidation kinetics of the SiC_p/ZC63 composite. The oxidation rate increased with increasing oxidation temperature, as expected. Especially, a drastic increase in the oxidation rate with increasing the temperature from 450 °C to 470 °C occurred. In Fig. 3, the oxidation at 470 °C was performed only for a short time to avoid ignition that can suddenly take place on the surface. The addition of Cu and Zn to Mg increases the oxidation rate of Mg [16], but the addition of SiC_p to Mg reduces the total surface area of the sample exposed to air, and thereby improves the oxidation resistance of SiC_p/ZC63 [17]. However, this beneficial effect was limited in the Mg alloys because the MgO scale is not inherently protective for the following reasons. (1) The MgO scale cannot cover the whole sample surface because its Pilling-Bedworth ratio is 0.81, and thereby does not act as a barrier to oxidative attack. (2) The vapor pressure of Mg and MgO keep increasing as

Table 2. Linear oxidation rate constant, k_l ($mg \cdot cm^{-2}h^{-1}$), of the SiC_p/ZC63 and SiC_p/AZ91D composites in air

Temperature (°C)	k_l of SiC_p/ZC63	k_l of SiC_p/AZ91D [17]
390	0.003	-
410	0.005	-
430	0.03	0.005
450	0.45	0.27
470	22.9	-

the temperature increases. (3) Oxidation of Mg to MgO is an exothermic reaction that gives off a large amount of heat. Hence, initially thin, adherent MgO scales soon become highly porous and poorly adherent at high-temperatures, eventually leading to ignition. At high temperatures, the MgO layer is entirely nonprotective, leading to ever increasing linear oxidation rates. Table 2 lists the linear oxidation rate constants, k_l, of SiC_p/ZC63. For the purpose of comparison, the k_l values of the AZ91D alloy (Mg-8.8Al-0.7Zn-0.22Mn in wt.%) with 10 wt.%SiC_p, viz., the SiC_p/AZ91D composites, are also listed in Table 2 [17]. The k_l values were calculated using the equation, $\Delta W = k_l \cdot t$, where ΔW was the weight gain per unit area and t the oxidation time. When calculating k_l, the initial, transient oxidation stage was excluded. The k_l values of SiC_p/ZC63 were larger than those of SiC_p/AZ91D, due to low oxidation resistance of Zn and Cu in ZC63.

Figure 4 shows the AES depth profiles of the oxidized SiC_p/ZC63. In order to investigate the oxidation mechanism, a thin Pd layer was sputter-deposited on the sample surface prior to oxidation. Palladium is a noble metal that does not oxidize. The maximum concentration point of Pd indicates the original sample surface. From the location of

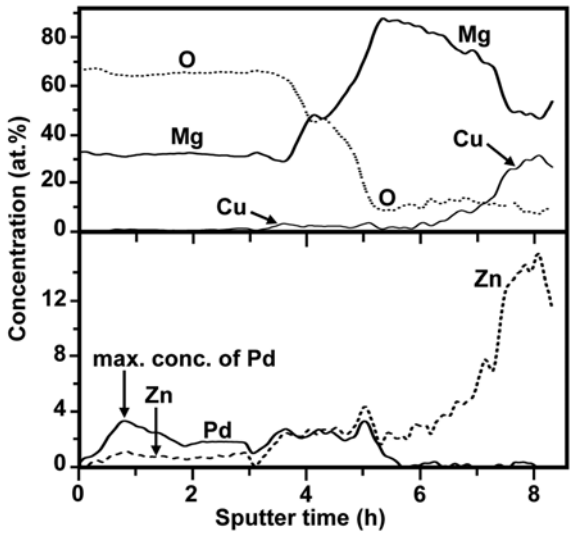

Fig. 4. AES depth profiles of SiC_p/ZC63 after oxidation at 410 °C for 30 min. The penetration rate is 23 nm/min for the reference SiO_2.

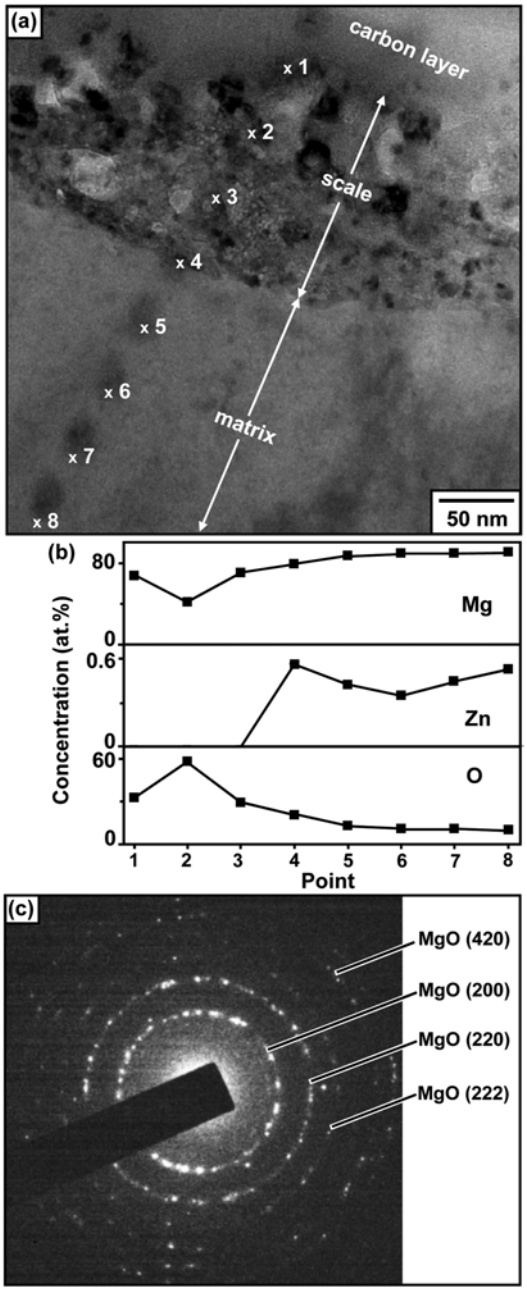

Fig. 5. TEM/EDS analyses of SiC_p/ZC63 after oxidation at 410 °C for 5 h. (a) cross-sectional image, (b) EDS lines profiles along points 1-8 shown in (a), and (c) SAED pattern of the oxide scale.

the Pd marker, it is seen that most of the oxide scale formed by the inward diffusion of oxygen. Oxygen can diffuse inwardly toward the oxide/matrix interface via imperfections or defects in the oxide scales. The outermost scale formed by the outward diffusion of a large amount of Mg and a small amount of Zn to the oxide/gas interface. This is consistent with the fact that MgO and ZnO grow by the outward diffusion of caions via the vacancy mechanism and the interstitial mechanism, respectively [18].

Figure 5 shows the TEM analytical results performed on the oxidized SiC_p/ZC63. In Fig. 5(a), a compact oxide film with a thickness of about 120 nm was seen. In Fig. 5(b), points 1 to 3 correspond to the MgO oxide layer, and points 4 to 8 correspond to the oxygen-affected zone where the concentration of oxygen decreased from 20.3 at.% to 9.3 at.%. Unlike in Fig. 4, Zn was absent in the oxide scale. Zinc was not intensively incorporated in the oxide scale due mainly to its small amount when compared with Mg. The selected area electron diffraction (SAED) pattern shown in Fig. 5(c) indicates that the MgO film consisted of randomly oriented nanocrystalline oxide grains. Under a mild oxidizing condition, such as oxidation at 410 °C for 5 h, the thin, dense MgO film formed may act as a diffusion barrier between the matrix and oxidizing gases. As the film thickens, tensile stresses will crack the oxide film partially at a certain critical thickness due to the unfavorable Pilling-Bedworth ratio of MgO, allowing easy access of atmospheric oxygen to the matrix surface. When cracks form, Mg gas transports through the oxide layer due to its high pressure vapor, and reacts directly with the oxygen. As a result, the initial protective stage shortens gradually with increasing the oxidation temperature.

Figure 6 shows the analytical results of the SiC_p/ZC63 composite after oxidation at 470 °C for 5 h. Under this severe oxidation condition, about a 250 μm-thick oxide layer formed (Fig. 6(a)). This thick oxide layer consisted of loosely adherent, numerous fine oxide crystallites (Fig. 6(b)). The top-view of the oxide layer is shown in Fig. 6(c), which displays the highly porous MgO scale. Oxygen penetrates inwards easily through the highly porous, loosely adherent, fine oxide crystallites. Then, the oxide layer is no longer an effective diffusion barrier to protect the matrix. In Fig. 6(a), the thermally stable SiC_p was scattered in the oxide layer and the matrix. The fact that SiC_p is located inside the oxide layer confirms that the oxidation progresses predominantly by the inward diffusion of anions such as oxygen and nitrogen. Figure 6(d) shows the optical micrograph of the matrix after etching with a solution of acetic acid: ethyl alcohol = 1: 15 (in volume). In Fig. 6(d), small, dark particles formed along the grain boundaries of the α-Mg matrix. The grain boundaries were enlarged in Fig. 6(e). The corresponding EDS analysis shown in Fig. 6(f) indicates that they were the Mg-Zn-Cu compound, which must be related with the CuMgZn compound outlined in Figs. 1 and 2. In Fig. 6(f), the Au and Pd peaks are due to (Au,Pd)-sputtering performed for SEM analysis. The Mg-Zn-Cu compound identified in Fig. 6(f) is presumed to be $Mg(Zn,Cu)_2$ [1,5,10,11] or Mg(Zn,Cu) [1] or Mg_2Zn_3 [4,5], which was previously identified from microstructural studies on Mg-Zn(-Cu) alloys. The CuMgZn compound identified in Figs. 1(e) and 2(a) decomposed into an α-Mg solid solution and Mg-Zn-Cu compound, owing to heating during oxidation.

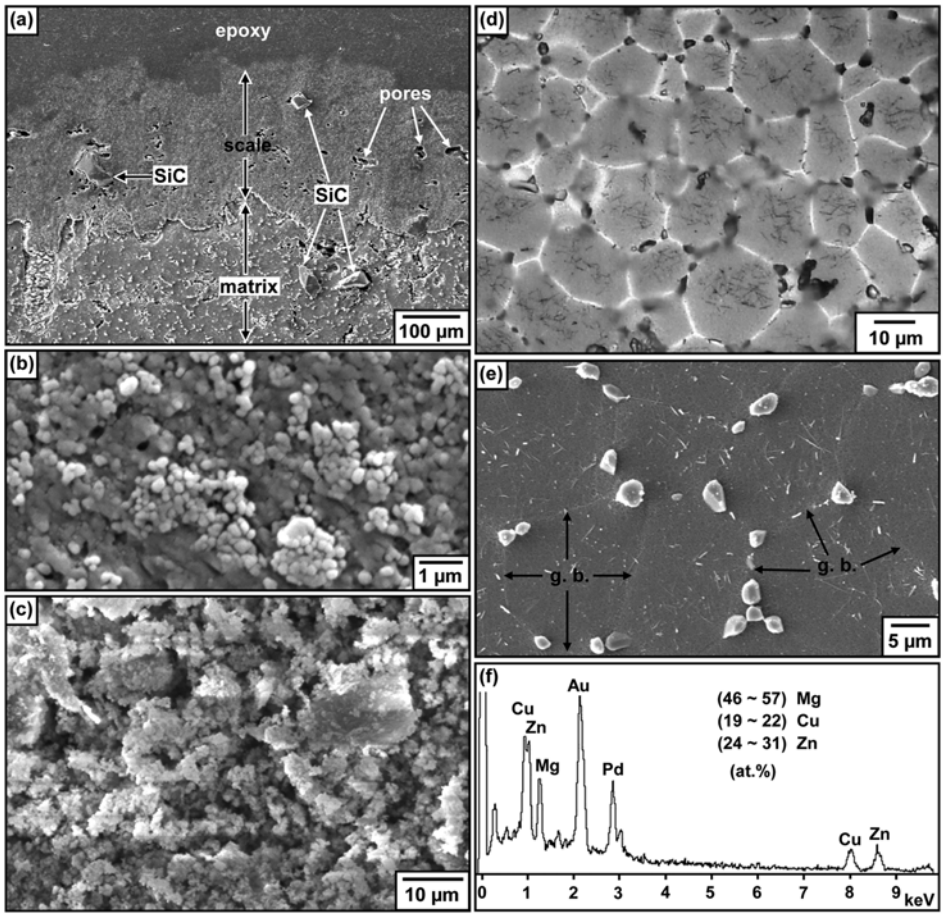

Fig. 6. SiC_p/ZC63 composite after oxidation at 470 °C for 5 h. (a) SEM cross-sectional image (etched), (b) enlarged SEM cross-sectional image of the oxide layer, (c) SEM top view of the oxide layer, (d) optical microstructure of the matrix (etched), (e) SEM image of the matrix (etched), and (f) EDS spectrum of small precipitates.

This may be the reason for the absence of the CuMgZn pattern in Fig. 2(b).

4. CONCLUSION

A SiC_p/ZC63 composite was cast and oxidized at 390 °C to 500 °C in air. The cast microstructure consisted of α-Mg matrix, SiC_p, and CuMgZn. During oxidation, the CuMgZn compound decomposed into an α-Mg solid solution and Mg-Zn-Cu compound. The oxidation rate began to increase sharply above 450 °C. The oxide layer consisted primarily of fine MgO grains and grew predominantly via the inward diffusion of oxygen. Mg and Zn did not diffuse outward much. The Initially formed, thin oxide scale later became thick, porous, and non-adherent at higher temperatures.

ACKNOWLEDMENT

This work is the outcome of "Environment-friendly and Energy-efficient Manufacturing Technology of Eco-Mg" program of KEIT grant funded by the Korea government Ministry of Knowledge Economy.

REFERENCES

1. J. H. Jun, J. M. Kim, B. K. Park, K. T. Kim, and W. J. Jung, *J. Mater. Sci*. **40**, 2659 (2005).
2. B. S. Shin, Y. Kim, and D. H. Bae, *J. Kor. Inst. Met. & Mater.* **46**, 1 (2008).
3. J. J. Jeon, S. W. Lee, B. H. Kim, B. G. Park, Y. H. Park, and I. M. Park, *J. Kor. Inst. Met. & Mater.* **46**, 304 (2008).
4. J. Buha, *Mater. Sci. Eng. A* **489**, 127 (2008).
5. O. J. Polmear, *Mater. Sci. Technol*. **10**, 1 (1994).
6. Z. Trojanová and P. Lukác, *Arch. Mater. Sci. Eng*. **28**, 361 (2007).
7. B. S. Shin, J. W. Kwon, and D. H. Bae, *Met. Mater. Int*. **15**, 203 (2009).
8. K. B. Lee, J. H. Choi, and H. Kwon, *Met. Mater. Int*. **15**, 33 (2009).
9. H. Z. Ye and X. Y. Liu, *J. Mater. Sci*. **39**, 6153 (2004).

10. B. Inem and G. Pollard, *J. Mater. Sci*. **28**, 4427 (1993).
11. W. Yang, G. C. Weatherly, D. W. McComb, and D. J. Lloyd, *J. Microscopy* **185**, Pt 2, 292 (1997).
12. F. Czerwinski, *Acta mater.* **50**, 2639 (2002).
13. J. Kiehn, M. Eilers, and K. U. Kainer, in *Magnesium Alloys and Their Applications*, ed. B. L. Mordike, and K. U. Kainer, p. 235, Hamburg, Germany, Werkstoff-informations Gesellshaft (1998).
14. C. M. Zhang, X. Hui, Z. G. Li, and G. L. Chen, *Mater. Lett*. **62**, 1129 (2008).
15. C. M. Zhang, X. Hui, K. F. Yao, Z. G. Li, and G. L. Chen, *Mater. Sci. Eng. A* **491**, 470 (2008).
16. T. E. Leontis and F. N. Rhines, *Trans. A.I.M.E.* **166**, 265 (1946).
17. T. D. Nguyen, J. C. Lee, S. J. Kim, Y. J. Kim, and D. B. Lee, *Surf. Rev. Lett.* **17**, 9 (2010).
18. N. Birks, G. H. Meier, and F. S. Pettit, *Introduction to the High-Temperature of Metals*, *2nd ed.*, p. 55, Cambridge University Press, UK (2006).